The Cryosphere Discuss., https://doi.org/10.5194/tc-2017-197
Manuscript under review for journal The Cryosphere
Discussion started: 10 October 2017

The Cryosphere Discussions
Open Access
EGU

Thermodynamic and Dynamic Ice Thickness Changes in the Canadian Arctic Archipelago in NEMO-LIM2 Numerical Simulations

Xianmin Hu[1], Jingfan Sun[1,+], Ting On Chan[1,++], and Paul G. Myers[1]

[1]Department of Earth and Atmospheric Sciences, University of Alberta, Edmonton, T6G 2E3, Canada
[+]summer intern from Zhejiang University, 38 Zheda Road, Hangzhou, China, 310027
[++]now at Skytech Solutions Ltd., Canada

Correspondence to: Xianmin Hu(xianmin@ualberta.ca)

Abstract. Sea ice thickness evolution within the Canadian Arctic Archipelago (CAA) is of great interest. In this study, based on the NEMO numerical frame work including the LIM2 sea ice module, simulations at both $1/4°$ and $1/12°$ horizontal resolution were conducted from 2002 to 2016. The model captures well the general spatial distribution of ice thickness in the CAA region, with very thick sea ice ($\sim 4m$ and thicker) in the northern CAA, thick sea ice ($2.5m$ to $3m$) in the west-central Parry Channel and M'Clintock Channel, and thin ($< 2m$) ice (in winter months) on the east side of CAA (e.g., eastern Parry Channel, Baffin Islands coast) and water channels in southern areas. Even though the configurations still have resolution limitations in resolving the exact observation sites, simulated ice thickness compares well with weekly Environment and Climate Change Canada (ECCC) New Icethickness Program data at nearby sites except in the north. At $1/4°$ to $1/12°$ scale, model resolution does not play a significant role in the sea ice simulation except to improve local dynamics because of better coastline representation. Sea ice growth is decomposed into thermodynamic and dynamic (including all non-thermodynamic processes in the model) contributions to study the ice thickness evolution. Relatively smaller thermodynamic contribution to ice growth between December and the following April is found in the thick and very thick ice regions, with larger contributions in the thin ice covered region. Wavelet analysis of the hourly simulated ice fields clearly shows the thermodynamic contribution have seasonal and diurnal cycles while only the seasonal cycle is significant for the total ice thickness. High frequency changes are found in both fields during the sea ice melting and formation process, particularly in the melting season.

1 Introduction

The Canadian Arctic Archipelago (CAA), the complex network of shallow-water channels adjacent to the Arctic ice pack, has been a scientific research hot spot for a long time. Scientifically, it is an important pathway delivering cold fresh Arctic water downstream (e.g., Prinsenberg and Hamilton, 2005; Melling et al., 2008; Dickson et al., 2007; Peterson et al., 2012), that eventually feeds the North Atlantic Ocean, where the watermass formation and ocean dynamics play a key role in the large scale meridional overturing circulation (MOC) and global climate variability (e.g., Rhein et al., 2011; Hátún et al., 2005; Marshall et al., 2001; Vellinga and Wood, 2002). Economically, under the context that Northern Hemisphere sea ice cover has

The Cryosphere Discuss., https://doi.org/10.5194/tc-2017-197
Manuscript under review for journal The Cryosphere
Discussion started: 10 October 2017

been declining dramatically (e.g., Parkinson et al., 1999; Serreze et al., 2007; Parkinson and Cavalieri, 2008; Stroeve et al., 2008; Comiso et al., 2008; Parkinson and Comiso, 2013), especially since 2007, shipping through the CAA , via the Northwest Passage (NWP), is of particular interest to commercial transport between Europe and Asia because of the great distance savings compared to the current route through the Panama Canal (e.g., Howell et al., 2008; Pizzolato et al., 2016, 2014). Besides the harsh weather and other security issues (e.g., icebergs), the biggest concern for the opening of the NWP is still the condition of sea ice, especially high concentrations of thick multiyear ice (MYI) (Melling, 2002; Howell et al., 2008; Haas and Howell, 2015).

Lietaer et al. (2008) estimated about 10% of the total Northern Hemisphere sea ice is stored within the CAA. Sea ice within the CAA region is a combination of both first-year ice (FYI) and MYI. MYI is both locally formed and imported from the Arctic Ocean, and normally located in the central-west Parry Channel and the northern CAA (e.g., Melling, 2002; Howell et al., 2008, 2013). Since the late 1970s, the ice free season has extended by about one week per decade (Howell et al., 2009), with a statistically significant decrease of 8.7% per decade in the September FYI cover. Reduction in the MYI cover is also found (-6.4% per decade) but not "yet statistically significant" due to the inflow of MYI from the Arctic Ocean mainly via the Queen Elizabeth Islands (QEI) gates in August to September (Howell et al., 2009, 2013). Even though the Arctic Ocean ice pack also extends to the CAA region through M'Clure Strait, the net sea ice flux is small and usually leads to an outflow from the CAA (Kwok, 2006; Agnew et al., 2008; Howell et al., 2013).

Although there is increasing demand for sea ice thickness information within this region, there is still very limited records available (Haas and Howell, 2015). Melling (2002) analyzed drill-hole data measured in winters during 1971–1980 within the Sverdrup Basin (the marine area between Parry Channel and QEI gates, see Fig. 1), and found sea ice in this region is landfast (100% concentration) for more than half of the year (from October-November to late July) with a mean late winter thickness of 3.4 m. Sub-regional means of the ice thickness can reach 5.5 m, but very thick multiyear ice was found to be less common, which is likely due to the melting caused by tidally enhanced oceanic heat flux in this region (Melling, 2002). The seasonal export of the old ice from the Sverdrup Basin down to south was known in the past (Bailey, 1957), which helps to create another major region with severe MYI condition in the CAA, the central Parry Channel and M'Clintock Channel (see Fig. 1 for the location). Based on two airborne electromagnetic (AEM) ice thickness surveys conducted in May 2011 and April 2015, Haas and Howell (2015) estimated the ice thickness to be 2 to 3 m in this region with MYI thicker than 3 m on average. This supports the general spatial distribution of ice thickness within the CAA, thicker in the north and relatively thinner in the south.

Observations were not only limited in time but also in spatial coverage, thus, numerical simulations are required to better understand the ice distribution and variability in the CAA (e.g., Dumas et al., 2006; Sou and Flato, 2009; Hu and Myers, 2014). Dumas et al. (2006) evaluated of the simulated ice thickness at CAA meteorological stations but with a uncoupled one dimensional (1D) sea ice model (Flato and Brown, 1996). The variability and trends of landfast ice thickness within the CAA were systematically studied by a recent paper from Howell et al. (2016) based on historical records at observed sites (Cambridge Bay, Resolute, Eureka and Alert) and numerical model simulations over the 1957–2014 period. They found statistically significant thinning at the sites except at Resolute, and this downward trend is mostly associated with the changes in snow depth. Although some of the numerical simulations used in Howell et al. (2016) produced a reasonable seasonal cycle, gen-

The Cryosphere Discuss., https://doi.org/10.5194/tc-2017-197
Manuscript under review for journal The Cryosphere
Discussion started: 10 October 2017

erally, these simulations overestimated ice thickness and did not do a good job in capturing the trend. In addition, the lack of horizontal resolution in these models were also pointed out in Howell et al. (2016).

In this paper, we will focus on the simulated CAA sea ice thickness over recent years (2002–2016), and address the skill of a sea ice model, including but not limited to those mentioned in Howell et al. (2016). To be more specific, this paper will discuss 1) the relative importance of thermodynamic and dynamic processes in sea ice growth/melting in simulating the possible variability of sea ice and ocean surface fields in the CAA; 2) high frequency changes in ice growth/melting processes. This paper starts with a brief description of the numerical simulations and observational data used in this study. Then the evaluation of simulated ice thickness in the CAA region is presented in section 3.1. The spatial distribution and temporal evolution (at selected sites) of thermodynamic and dynamic ice thickness change are discussed in section 3.2. Section 3.3 focuses on the high frequency (up to diurnal cycle) variability in ice growth/melting processes. Concluding remarks and a discussion are given in section 4.

The Cryosphere Discuss., https://doi.org/10.5194/tc-2017-197
Manuscript under review for journal The Cryosphere
Discussion started: 10 October 2017

2 Method and Data

2.1 Numerical model setup

In this study, the coupled ocean sea ice model, the Nucleus for European Modeling of the Ocean (NEMO, available at https://www.nemo-ocean.eu) version 3.4 (Madec and the NEMO team, 2008), is utilized to conduct the numerical simulations. The model domain covers the Arctic and the Northern Hemisphere Atlantic (ANHA) with two open boundaries, one close to Bering Strait in the Pacific Ocean and the other one at 20°S across the Atlantic Ocean (Fig. 1, inset). The model mesh is extracted from the the global tripolar grid, ORCA (Drakkar Group, 2007) with two different horizontal resolutions, 1/4° (hereafter ANHA4) and 1/12° (hereafter ANHA12). The highest horizontal resolution is $\sim 2\,km$ for ANHA12 and $\sim 6\,km$ for ANHA4 in Coronation Gulf–Dease Strait region, which is near the artificial pole over northern Canada (Fig. 1), and the lowest resolution is $\sim 9\,km$ for ANHA12 and $\sim 28\,km$ for ANHA4 at the equator. In the vertical, there are 50 geopotential levels with high resolution focused in the upper ocean. Layer thickness smoothly transitions from $\sim 1m$ at surface (22 levels for the top $100\,m$) to $458\,m$ at the last level.

The sea ice module used here is the Louvain la-neauve Ice Model Version 2 (LIM2) with an elastic-viscous-plastic (EVP) rheology (Hunke and Dukowicz, 1997), including both thermodynamic and dynamic components (Fichefet and Maqueda, 1997). It is based on a three-layer (one snow layer and two ice layers of equal thickness) model proposed by Semtner Jr (1976) with two ice thickness categories (mean thickness and open water). The sea ice module is coupled to the ocean module every model step. The elastic time scale is tuned small enough to damp the elastic wave in the EVP approach (see Table 1), based on the discussions in Hunke and Dukowicz (1997). A no-slip boundary condition is applied for sea ice in the simulations, which means the ice can have zero velocity along the coast. However, it should be noted that the sea ice module used in this study does not include a representation of landfast ice (e.g., Lemieux et al., 2016), which may negatively impact the sea ice simulation where landfast ice exists.

Table 1. Sea ice module parameters used in our simulations

parameter	ANHA4	ANHA12
time step (seconds)	1080	180
subsycling iterations	150	120
timescale of elastic wave (seconds)	320	60

Two simulations, ANHA4-CGRF and ANHA12-CGRF, are integrated from January 1st 2002 to December 31 2016. The initial conditions, including three dimensional (3D) ocean fields (temperature, salinity, zonal velocity and meridional velocity) as well as two dimensional (2D) sea surface height (SSH) and sea ice fields (concentration and thickness) are taken from from the Global Ocean Reanalysis and Simulations (GLORYS2v3) produced by Mercator Ocean (Masina et al., 2015). Open boundary conditions (temperature, salinity and horizontal ocean velocities) are derived from the monthly GLORYS2v3 product as well. At the surface, the model is driven with high temporal (hourly) and spatial resolution ($33\,km$) atmospheric forcing data

The Cryosphere Discuss., https://doi.org/10.5194/tc-2017-197
Manuscript under review for journal The Cryosphere
Discussion started: 10 October 2017

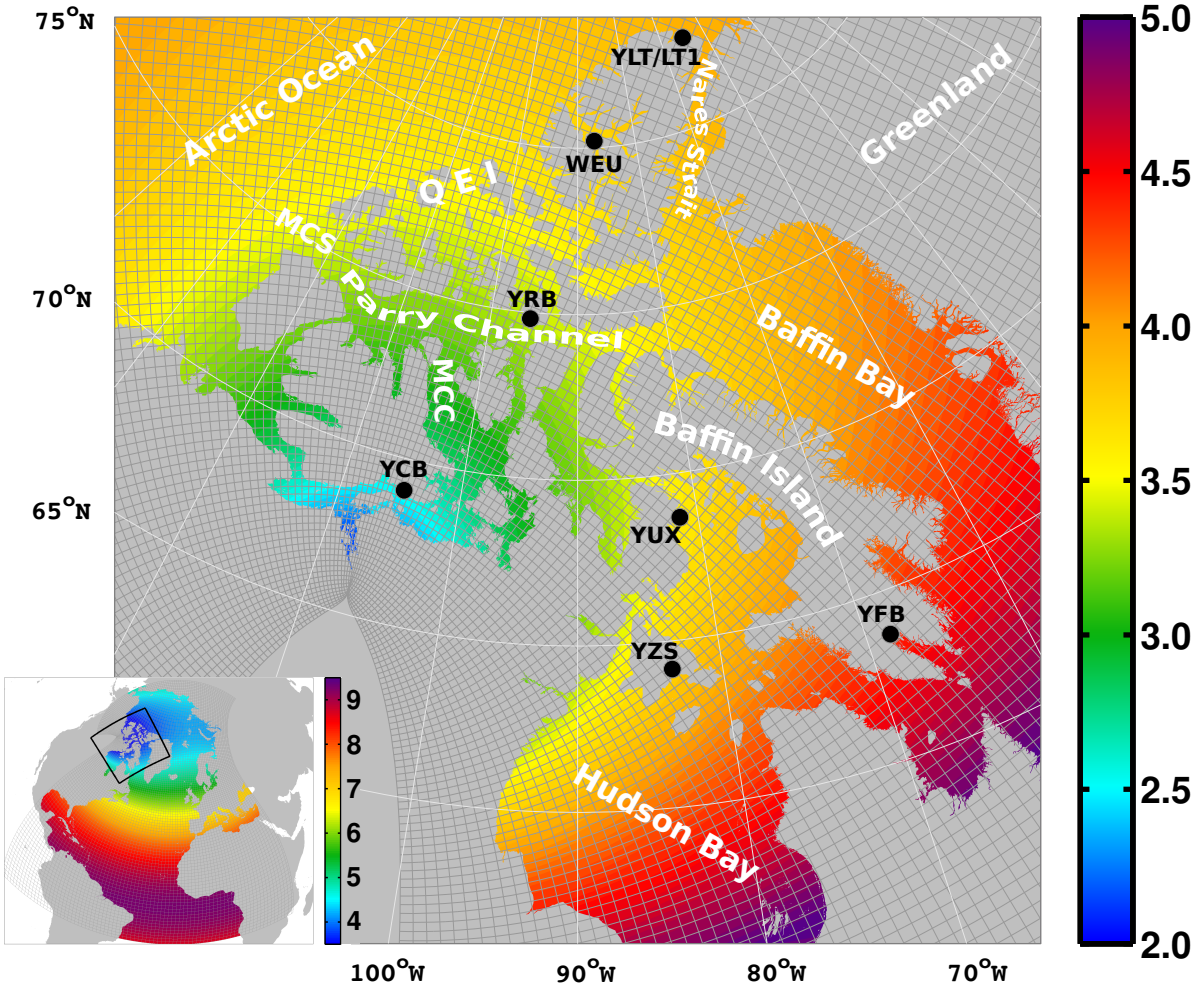

Figure 1. ANHA12 (inset) model mesh (every 10th grid point) and horizontal resolution (colours, unit: kilometers) in the Canadian Arctic Archipelago (QEI: Queen Elizabeth Islands; MCS: M'Clure Strait; MCC: M'Clintock Channel) and Hudson Bay region (thick black box highlighted in the inset). Note the colour scale is different from that used in the inset). Ice thickness observation sites (see table 2 for the details) are shown with black circles on the map.

provided by Canadian Meteorological Centre (CMC) Global Deterministic Prediction System (GDPS) ReForecasts (CGRF) dataset (Smith et al., 2014), including 10 m wind, 2 m air temperature and humidity, downwelling and longwave radiation flux, and total precipitation. Inter-annual monthly $1^\circ \times 1^\circ$ river discharge data from Dai et al. (2009) as well as Greenland meltwater ($5\,km \times 5\,km$) provided by Bamber et al. (2012) is carefully (volume conserved) remapped onto the model grid.

With the same setting as ANHA4-CGRF but driven with the inter-annual atmospheric forcings from the Coordinated Ocean-ice Reference Experiments version 2 (CORE-II) (Large and Yeager, 2009), another ANHA4 simulation, ANHA4-CORE, integrated from January 1st 2002 to December 31 2009, is also conducted to study the sensitivity of the sea ice simulation to the

The Cryosphere Discuss., https://doi.org/10.5194/tc-2017-197
Manuscript under review for journal The Cryosphere
Discussion started: 10 October 2017

atmospheric forcings. The CORE-II provides fields at various temporal resolutions, a) 6-hourly 10-m surface wind, 10-m air temperature and specific humidity; b) daily downward longwave and shortwave radiation; c) monthly total precipitation and snowfall.

No temperature or salinity restoring is applied in any of the simulations used in this study. Without such constrains the model evolves freely in time to help understand better the limitations of the physical processes represented by the model.

Monthly ice thickness at $1/4^\circ$ resolution from the GLORYS2v3 product with sea ice assimilation is also utilized in this study to better understand the initial condition issue.

2.2 Environment and Climate Change Canada New Arctic Ice Thickness Program

To evaluate the performance of the model in terms of ice thickness, simulated ice thickness is compared to the observed data from Environment and Climate Change Canada (ECCC) New Icethickness Program (hereafter ECCC thickness). The new ECCC thickness program, the second stage of the Original Ice Thickness Program Collection used in Dumas et al. (2006), started in the fall of 2002 , and continued to the present at only 11 stations (including sites in lakes). Measurements were conducted weekly at approximately the same location close to shore between freeze-up and break-up period (when the ice was safe to walk on) with a special auger kit or a hot wire ice thickness gauge. Data is made available to the public by Environment and Climate Change Canada under the Open Government License (Canada) on http://open.canada.ca/data/en/dataset. Eight coastal sites, Carol Harbour (YZS), Hall Beach (YUX), Iqaluit (YFB), Cambridge Bay (YCB), Resolute (YRB), Eureka (WEU), Alert YLT (YLT) and Alert LT1 (LT1), were used in this study. The detailed location information of each site can be found in Fig. 1 and Table2.

Table 2. ECCC ice thickness station locations (only sites used in this study)

site	longitude	latitude
Carol Harbour (YZS)	$83.153^\circ W$	$64.130^\circ N$
Hall Beach (YUX)	$81.230^\circ W$	$68.780^\circ N$
Iqaluit (YFB)	$68.517^\circ W$	$63.726^\circ N$
Cambridge Bay (YCB)	$105.06^\circ W$	$69.113^\circ N$
Resolute Bay (YRB)	$94.884^\circ W$	$74.684^\circ N$
Eureka (WEU)	$85.942^\circ W$	$79.986^\circ N$
Alert LT1 (LT1)	$62.593^\circ W$	$82.602^\circ N$
Alert YLT (YLT)	$62.420^\circ W$	$82.753^\circ N$

Unlike the 1D model used in Dumas et al. (2006), which can be applied at the exact location where the measurements were carried out, three dimensional (3D) models usually have horizontal resolution issues in resolving the observation sites, even with the high resolution ANHA12 configuration used in this study. Interpolation is needed to do the comparison between simulated fields and observations. This is also mentioned in Howell et al. (2016). To interpolate simulated fields onto the

The Cryosphere Discuss., https://doi.org/10.5194/tc-2017-197
Manuscript under review for journal The Cryosphere
Discussion started: 10 October 2017

nearest water point (x_k, y_k) of each observation site (x_{obs}, y_{obs}), we utilized a modified inverse distance weighting (IDW) method (eq. (1)) proposed by Renka (1988):

$$f_i = [\frac{R_w - d_k}{R_w\, d_k}]^2 \tag{1a}$$

$$w_i = \frac{f_i}{\sum_{i=1}^{N} f_i} \tag{1b}$$

$$Q_{target} = \sum_{i=1}^{N} Q_i\, w_i \tag{1c}$$

where R_w is the influence radius about point (x_k, y_k), d_k is the distance from point (x_k, y_k) to each neighboring point (x_i, y_i), f_i is the inverse distance function, w_i is the weight function on each neighboring point (x_i, y_i), N is the number of neighboring points within R_w, Q_i is variable value on each neighboring point and Q_{target} is the final result. In practice, nine neighboring points, including point (x_k, y_k), were considered in the calculated. As R_w is set to the maximum value of d_k and land points should be excluded, eventually up to eight effective points are used in our interpolation process.

The Cryosphere Discuss., https://doi.org/10.5194/tc-2017-197
Manuscript under review for journal The Cryosphere
Discussion started: 10 October 2017

3 Results

In this section, first, the ice thickness reproduction ability within the CAA of the NEMO LIM2 configurations used in this study will be examined via comparisons with the ECCC thickness. Then the detailed thermodynamic and dynamic ice thickness changes, both the spatial distribution and temporal evolution at select sites (Cambridge Bay and Resolute Bay), based on the simulation outputs will be presented. Then, the high frequency ice growth/melting processes resolved by the simulation will be studied.

3.1 Ice thickness comparison

Figure 2 shows the ice thickness comparison with observations. In general, both ANHA4-CGRF (blue lines) and ANHA12-CGRF (red lines) simulations produce similar seasonal and inter-annual variations in ice thickness, which compare reasonably well at some sites (i.e., YCB, YZS, YUX, YRB,YFB) but not at the rest (WEU, YLT, LT1). Although the observations are missing in the sea ice melting season, an asymmetric seasonal cycle (a shorter faster melting period follows a relatively longer slow growth period), is evidenced by the available data, and reproduced by the simulations. Taking account of the model resolution, the interpolated simulated ice thickness reflects actually the variability some distance off the coast rather than the exact observation locations. The geographic location differences, which is also related to model resolution, could also lead to discrepancies in the comparisons here. Thus, if the model can capture the seasonal cycle (e.g., multiple data points in both ice growth and melting seasons), the model is likely capable of simulating the process.

At YFB, the model does a good job in most years but failed to catch the very thick sea ice in 2014, 2015 and 2016 (Fig. 2h). This could be a local atmospheric forcing field bias, or a model resolution issue, i.e., the measurements captured very localized extremes beyond the ability of model to resolve. Similar behavior happens at YZS, YUX. Further investigation is needed.

At WEU, YLT and LT1 sites (Fig. 2e, f, and g), there is a clear initial value issue ($\sim 2\,m$ at YLT/LT1 and $\sim 1\,m$ at MEU) that leads to too thick sea ice in the simulations. Note that neither ANHA4 or ANHA12 has the capability to resolve the difference between YLT and LT1, thus, the same simulated values are shown on the figure for both YLT and LT1. At YLT/LT1, both ANHA4-CGRF (blue line) and ANHA12-CGRF (red line) show similar inter-annual trends to that in GLORYS2v3 (which extends back to 1993, greenline), meaning it is likely a pure initial value problem rather than the model equilibrium issue mentioned in Howell et al. (2016). In addition, the seasonal cycle is not clear in the GLORYS2v3 product. The issue is also present in some years, i.e., 2005–2007, in the ANHA4-CGRF and ANHA12-CGRF simulations. ANHA4-CORE (orange line) is generally improved compared with the observations in both the amplitude and seasonal cycle. However, this improvement was achieved by accident, and is related to a snow depth issue in this simulation (more details will be in the discussion session). Thus, it does not indicate that CORE-II forcing is performing better than other atmospheric forcing datasets in this region. The equilibrium issue, i.e., ice thickness keep increasing, might happen at WEU in our simulations with either CGRF or CORE-II forcing. The upward trend over 2005 to 2007 is also present in the observations but is missing in the GLORYS2v3 although GLORYS2v3 has a small thickness (which is likely due to data assimilation or an atmospheric forcing issue in 2005). Its trend does not reflect the real change/variability

The Cryosphere Discuss., https://doi.org/10.5194/tc-2017-197
Manuscript under review for journal The Cryosphere
Discussion started: 10 October 2017

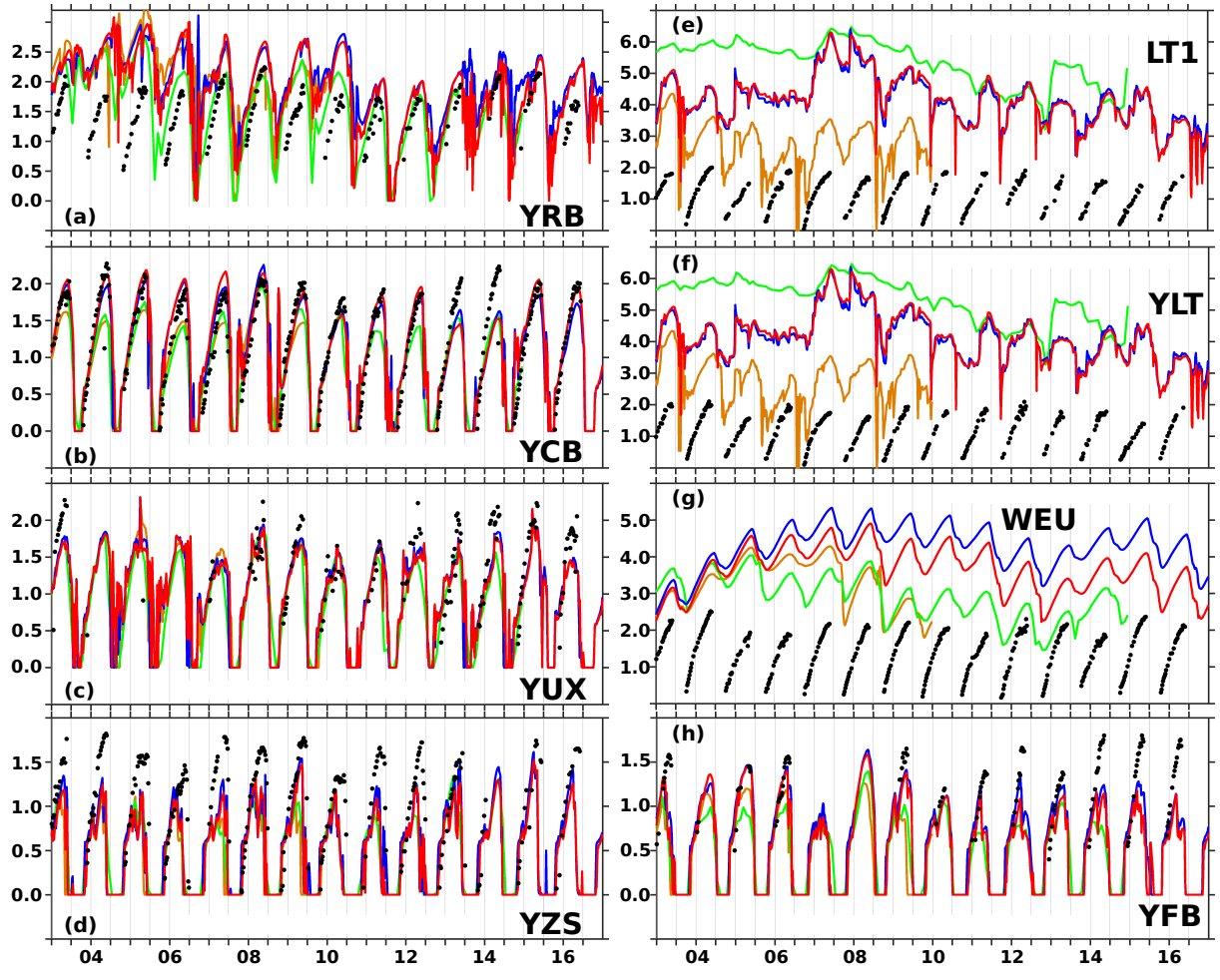

Figure 2. Simulated ice thickness at each selected ECCC thickness site (figure 1 and table 2, unit: meters) from January 2003 to December 2016 (orange: ANHA4-CORE simulation; green: GLORYS2v3 product; blue: ANHA4-CGRF simulation; red: ANHA12-CGRF simulation) against weekly ECCC observations (black dots). Note the GLORYS2v3 product is a monthly mean field while the rest of the simulations use 5-day averages.

At YCB, simulations (red and blue lines in Fig. 2b) with CGRF forcing show very good agreement with the observations except during the winters of 2013 and 2014. Considering the horizontal resolution of our simulations is not capable of resolving the inner bay at the Cambridge Bay, the match in ice thickness between the simulation and observations indicates the variation of ice thickness within the inner Bay might be small. Both ANHA4-CORE and GLORYS2v3 simulations underestimated the maximum values in winters by $\sim 0.5m$. This indicates CGRF forcings might provide more realistic surface inputs in this region.

The Cryosphere Discuss., https://doi.org/10.5194/tc-2017-197
Manuscript under review for journal The Cryosphere
Discussion started: 10 October 2017

At YRB, it is more complicated (Fig. 2a). Prior to the significant sea ice melting in 2007, none of the simulations show ice free conditions in this region in summer. GLORYS2v3 shows relatively thinner ice in summer months but it is still $0.5\,m$ to $1.5\,m$ thick. It could be the initial value problem. However, high frequently variations even in winter in the ANHA simulations suggest that the ice growth process is not dominated by a smoothly changing physical process (e.g., air temperature). Thus, it is likely due to the physical process (e.g., advection from surrounding areas). This will be discussed more in the following section. Post 2007, the seasonal cycle in the sea ice field is more distinct, although ice free summer conditions do not happen every year. After 2010, simulations produce winter sea ice thickness much close to the observations.

3.2 Thermodynamic and dynamic ice thickness change

In the real world, both the thermodynamic and dynamic ice thickness processes are coupled together (occurring at the same time). However, with the assistance of numerical model, the two processes can be decoupled (shown in equation (2)) to better understand the relative importance of each process.

$$\Delta H_{total} = \Delta H_{thermal} + \Delta H_{dynamic} \tag{2}$$

where ΔH_{total} is the total ice thickness change over a specific time interval; $\Delta H_{thermal}$ is the ice thickness change due to vertical heat fluxes (through the atmosphere-ice-ocean interfaces); $\Delta H_{dynamic}$ is the ice thickness change due to dynamic processes. In practice, a simple approach is utilized to compute the two terms on the right side. $\Delta H_{thermal}$ is calculated based on the model thermal ice production. $\Delta H_{dynamic}$ is taken as the residual from the ΔH_{total}.

3.2.1 Spatial distribution

Here we focus on ice growth process between December and April of the following year. Figure 3a and 3b show the simulated ice thickness in ANHA12 at the beginning of December and at the end of April, respectively. Geographically, at the end of April, a) very thick sea ice is located in the northern CAA ($\sim 4\,m$ by the end of April) with regional maximum ($> 4.5\,m$) at the openings to the Arctic Ocean. b) less thick sea ice covers western, and central Parry Channel (just above the site YRB) and M'Clintock Channel with a thickness of $2.5\,m$ to $3\,m$. c) relatively thin ice ($< 2\,m$) is mainly in the southern CAA, eastern Parry Channel, coasts of Baffin Islands and within Hudson Bay. Invasion of the Arctic Ocean ice pack through the northern CAA openings and the advection from there into central Parry Channel are clearly shown in the figures, consisted with previous studies (e.g., Melling, 2002; Howell et al., 2008; Haas and Howell, 2015).

During the winter, sea ice grows everywhere in the CAA regions due to the thermodynamic cooling (Fig. 3c). But the total increase over the winter is not evenly distributed in space. Nor is ice growth largest in the north. Large thermodynamic ice growth is seen in the eastern CAA (eastern Parry Channel, Nares Strait, Baffin Island coast and western Hudson Bay), Amundsen Bay and many coastal regions (e.g., western coast of Banks Island, northern coast of western Parry Channel). Regions covered by thick sea ice (i.e., the northern CAA, west-central Parry Channel and M'Clintock Channel) show less thermodynamic ice growth over the winter. This is particularly true in the northern CAA, likely due to the existence of already thick ice reducing the heat exchange between the ocean and atmosphere.

The Cryosphere Discuss., https://doi.org/10.5194/tc-2017-197
Manuscript under review for journal The Cryosphere
Discussion started: 10 October 2017

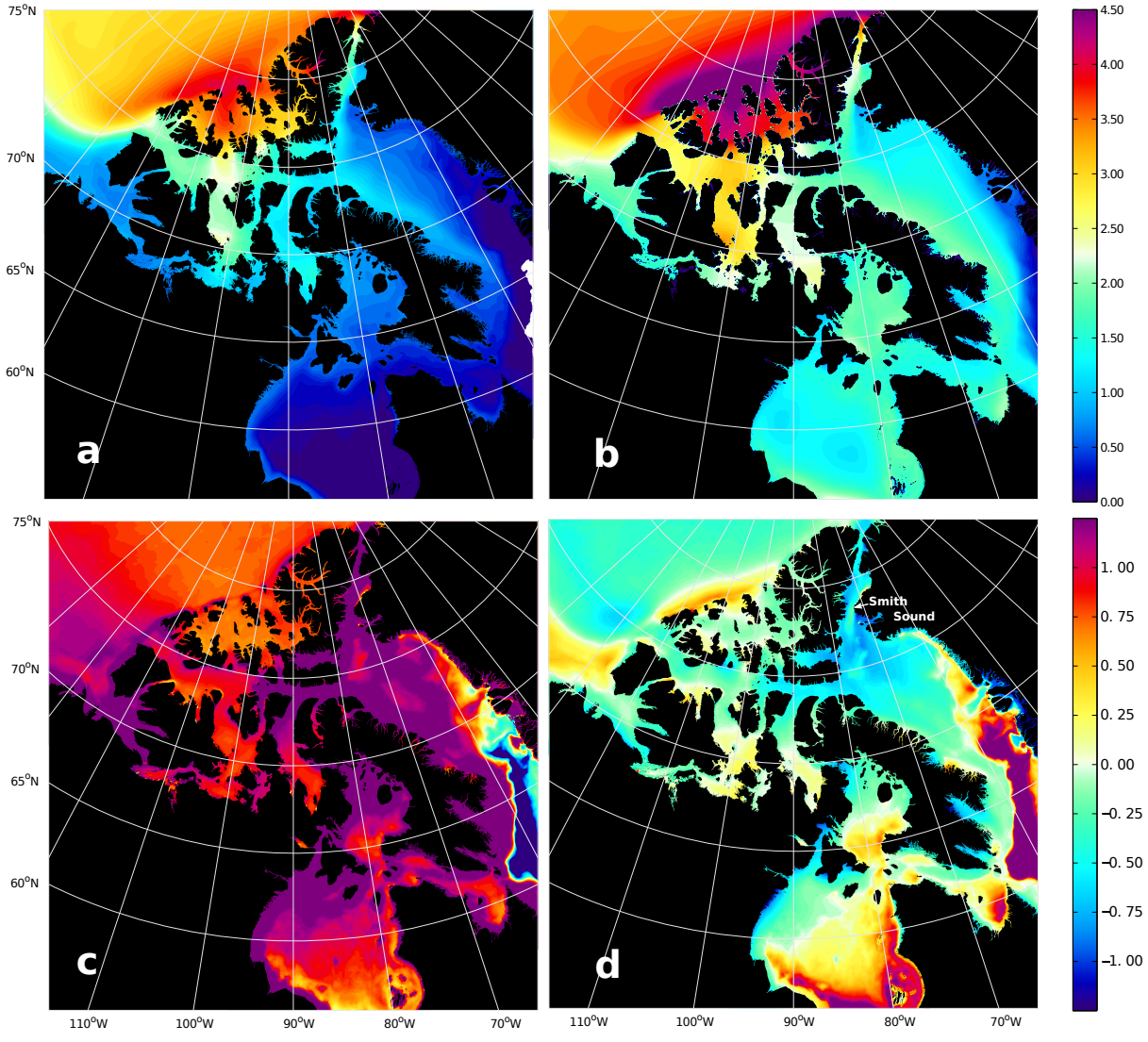

Figure 3. Upper panel shows the thickness (unit: meters) averaged over 2003–2016 at the beginning of December (a) and at end of April (b). Lower panel shows the thermodynamics component (c) and dynamic component ice thickness contribution (unit: meters) between December (a) and the following April (b) averaged over 2003-2015. ANHA12-CGRF simulation is used here.

The dynamic contribution to sea ice thickness is mainly negative (reduces local ice thickness) within the CAA (Fig. 3d). Large positive values (0.4 to $0.7\,m$) are shown along the Arctic Ocean coast off the CAA and within the Beaufort Sea. This is consistent with known sea ice convergence or strong advection of thick ice from upstream regions (Kwok, 2015; Maslanik et al., 2011). Within the northern CAA, west-central Parry Channel and M'Clintock Channel, there is ~ 0.25 thick ice loss locally due to the dynamics. Note the positive values occurring in the south of M'Clintock Channel, suggesting a net convergence

The Cryosphere Discuss., https://doi.org/10.5194/tc-2017-197
Manuscript under review for journal The Cryosphere
Discussion started: 10 October 2017

there which contributes to the local ice thickening in winter. In the eastern CAA (e.g., eastern Parry Channel, Nares Strait and northwest corner of Baffin Bay), there are large negative dynamic thickness contributions, implying strong ice advection.

Although the North Water (NOW) Polynya (e.g., Dunbar, 1969; Melling et al., 2001) region is still ice covered by the end of April (Fig. 3b), the spatail distribution of negative dynamic ice thickness (which helps to remove local ice) captures the shape of NOW Polynya well. Weaker advection of sea ice at Smith Sound and to its south, which is likely to be caused by ice jamming, is also simulated by the model.

3.2.2 Seasonal cycle at YCB and YRB

Two sites, YCB and YRB, were selected to further study the seasonal cycle of the thermodynamic and dynamic ice thickness changes.

Figure 4 shows the seasonal cycle of ice thickness, 5-day $\Delta H_{dynamic}$ and $\Delta H_{thermal}$ averaged between 2003 and 2016 at YCB. Sea ice reaches its maximal thickness ($\sim 2\,m$) in late May with ice free conditions for about two months (August and September). As the sea ice starts to form (October and November), both thermodynamics (e.g., due to cold temperature) and dynamics (e.g., local advection) play a role in the production of the ice thickness although with opposite contributions (Fig. 4b and c). Starting from December through to the end of the next May, it is almost a pure thermodynamic process that controls the ice thickness change. Note the thermodynamic ice production is not constant in time, it is about three times larger in the first period ($\sim 0.03 m\,per\,day$) than in the later period ($\sim 0.01\,m\,per\,day$). The steady thermodynamic growth in the second period contributes to about half of the total ice thickness. During the ice melting period (June and July), the thermodynamics is the major player as well (Fig. 4c).

At YRB, on average, there is no ice free period ($\sim 2.5\,m$ at the end of May and $\sim 1\,m$ in August and September) (Fig. 5a), albeit with large inter-annual variability (Fig. 2a). For example, in 2012, there is an ice free in the mid of September (Fig. 6a). The freeze-up date is about half a month earlier at YRB than that at YCB. The ice production is a little bit higher at the beginning (October to December), $\sim 0.02\,m\,per\,day$, than later (5b), $\sim 0.01\,m\,per\,day$, but the difference is not as noticeable as at YCB (Fig. 4b). The relatively faster thermal growth lasts longer at YRB than that at YCB, likely due to local advection. These features are also applicable to a specific year, e.g., 2012 (Fig. 6). The non-thermodynamic contribution is more significant than at YRB (Fig. 4c) but basically plays a negative role, i.e., slowing ice thickness increase during the winter season. Similarly to YCB, the thermodynamics is the dominant factor melting the sea ice, with a melting peak in July. During the melting season, more ice can be advected to YRB and melts later locally (Fig. 5c) than that at YCB (Fig. 4c).

3.3 High frequency thermodynamic processes during ice formation and melting

Constrained by sampling frequency in observations and atmospheric forcing data, very few modelling studies have ever studied ice thickness variations on a time scale shorter than monthly. Using a 1D thermodynamic sea ice model, Hanesiak et al. (1999) found the hourly atmospheric forcing, which resolves the diurnal cycle, can produce more realistic results in terms of sea ice melting processes (i.e., simulated breakup dates, open water duration and snow ablation) compared to the non-diurnal-resolved forcing (e.g., daily). The significant differences is caused by the nonlinearities in surface energy balance that affects the snow

The Cryosphere Discuss., https://doi.org/10.5194/tc-2017-197
Manuscript under review for journal The Cryosphere
Discussion started: 10 October 2017

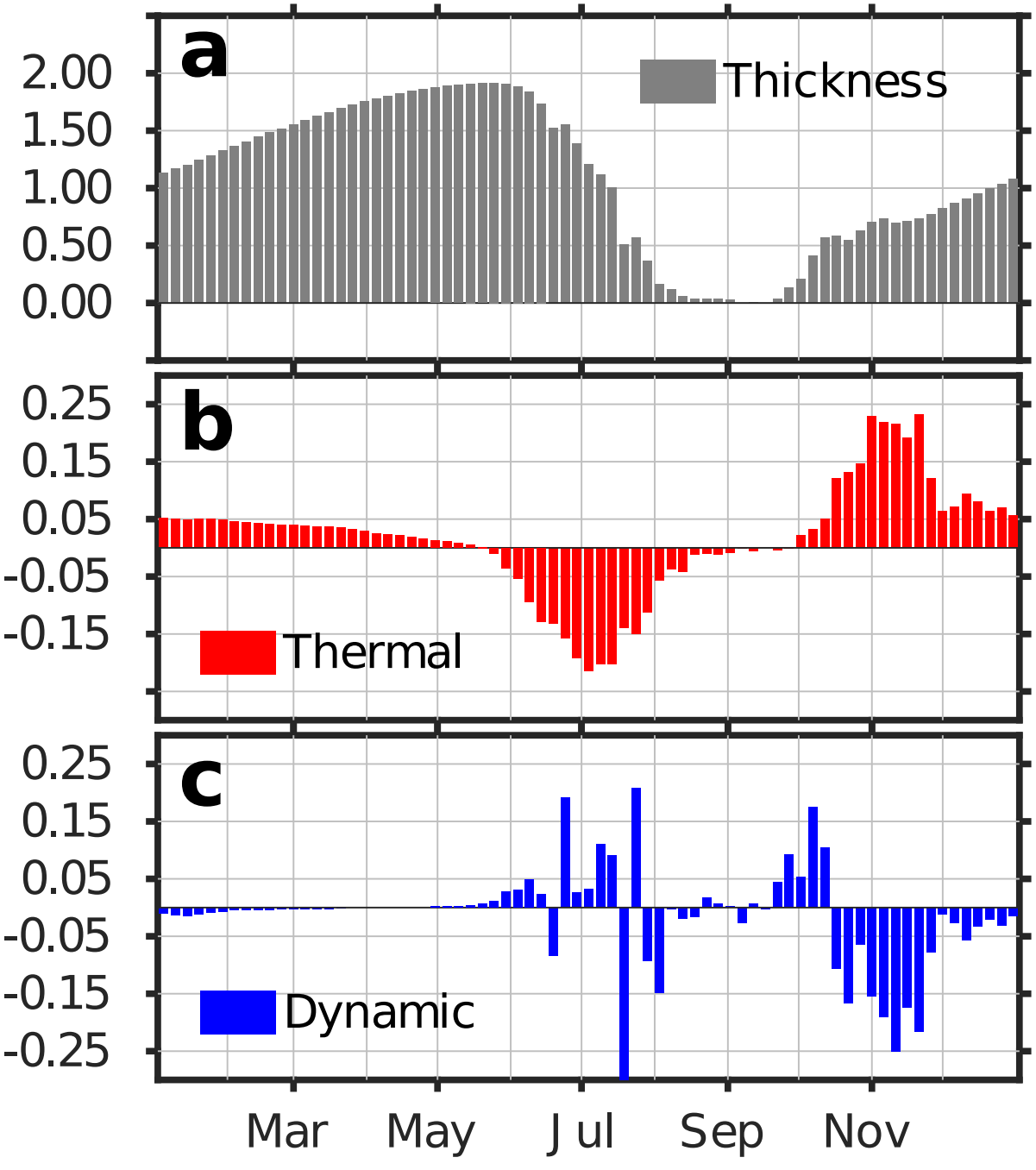

Figure 4. Seasonal cycle (averaged over 2003 to 2016) of ice thickness (a, unit:meters), dynamic (b) and thermodynamic (c) ice thickness changes (unit: meters per 5-day) at YCB from the ANHA12-CGRF simulation. Note each x-grid line indicates the beginning of each month.

The Cryosphere Discuss., https://doi.org/10.5194/tc-2017-197
Manuscript under review for journal The Cryosphere
Discussion started: 10 October 2017

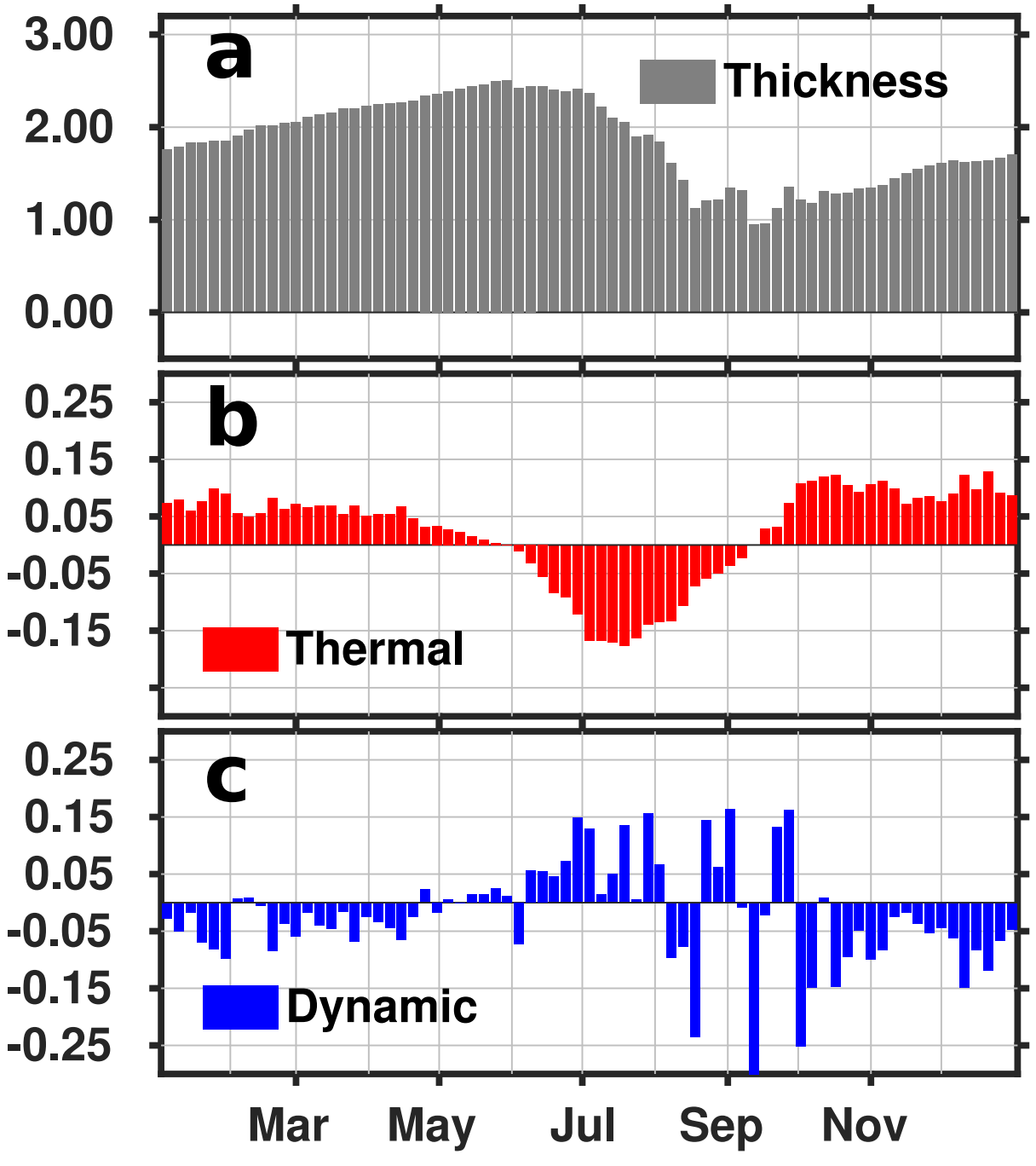

Figure 5. Same as Fig. 4 but at YRB.

depth, albedo and surface temperature (Hanesiak et al., 1999). Thus, in this study, more realistic sea ice melting and freezing processes are expected, given that the CGRF dataset provides hourly surface atmospheric forcing fields. Hourly simulated sea

The Cryosphere Discuss., https://doi.org/10.5194/tc-2017-197
Manuscript under review for journal The Cryosphere
Discussion started: 10 October 2017

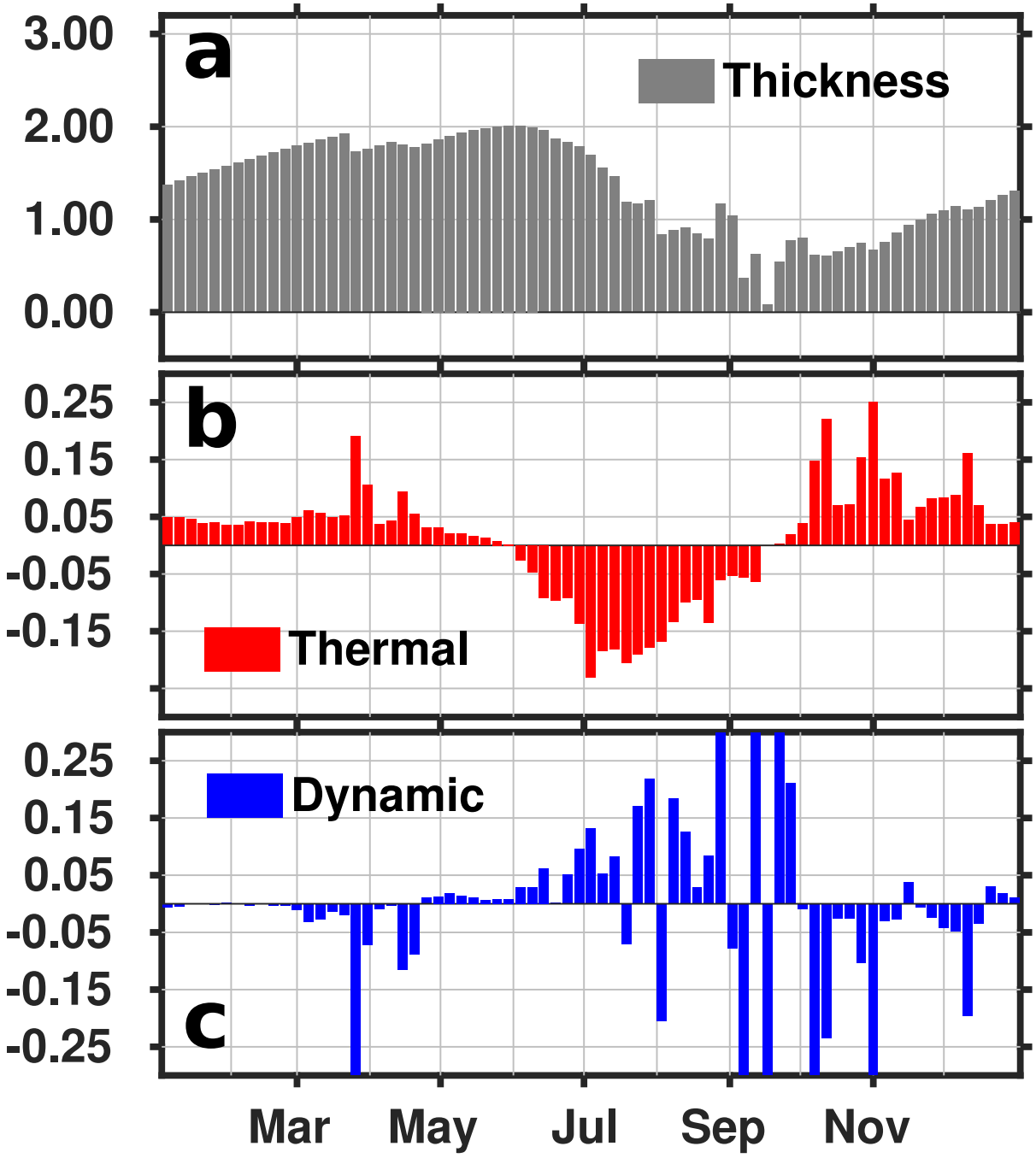

Figure 6. Same as Fig. 5 but only considered 2012 for ANHA12-CGRF.

ice fields (ice thickness, thermodynamic ice production) are saved from the ANHA12-CGRF simulation between 2008 and 2016 to further study the high frequency processes in ice thickness evolution. Wavelet analysis (Torrence and Compo, 1998) is

The Cryosphere Discuss., https://doi.org/10.5194/tc-2017-197
Manuscript under review for journal The Cryosphere
Discussion started: 10 October 2017

utilized to show both the periods of the ice thickness variation and their temporal evolution, The wavelet toolbox is accessible from http://paos.colorado.edu/research/wavelets, and a bias correction discussed in Veleda et al. (2012) is also included in our analysis.

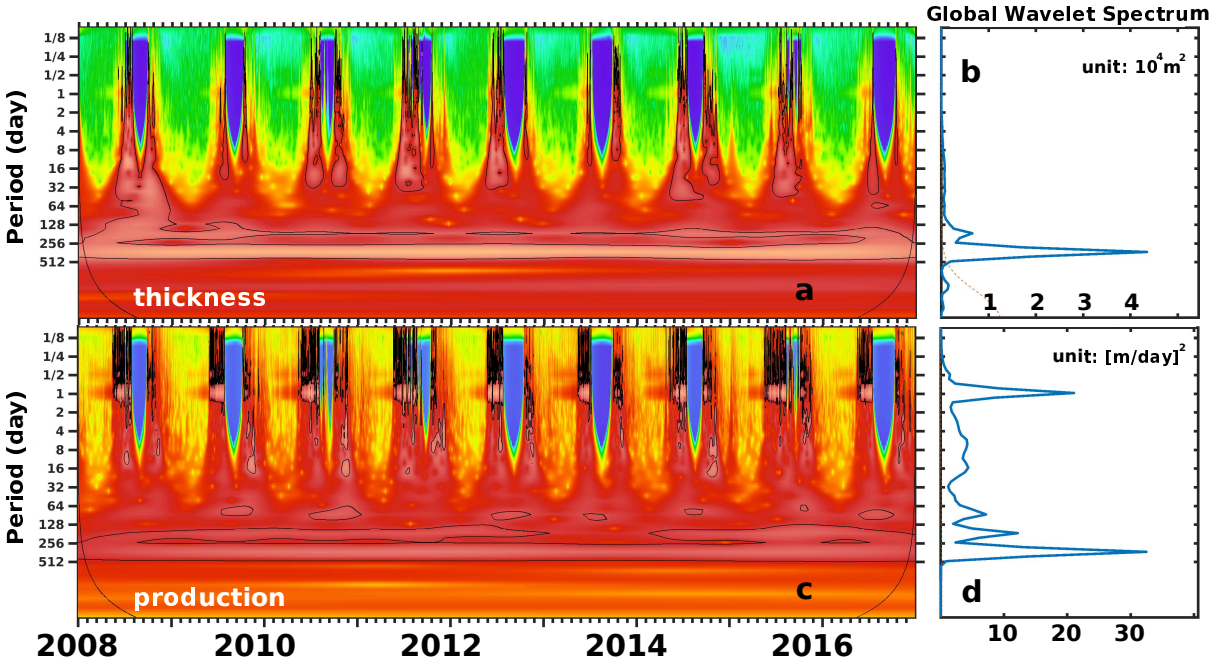

Figure 7. Wavelet spectrum (left, black contours highlight the significant oscillations at a confidence level of 95%) and global power spectrum (right) of ANHA12 hourly ice thickness (upper panel) and thermodynamic ice production (lower panel) at YCB

Figure 7 shows the wavelet spectrum (a and c) and the global wavelet spectrum (b and d) of the ice thickness (a and b) and ice thermodynamic production (c and d) at YCB. The thermodynamic ice production was converted to $m per day$ and normalized based on its standard deviation before performing the wavelet. The season cycle dominates the variability in all the years throughout the simulation period (2008 to 2016), which is also shown in the global wavelet spectrum (Fig. 7b). High frequency oscillations down to a period of a week are significant before and after the ice free period (Fig. 7a). This supports that the ECCC weekly sampling frequency is good enough during the ice break-up and freeze-up periods. The high frequency ice thickness variation is associated with the diurnal cycle in the thermal ice production (Fig. 7c). The wavelet of the non-thermodynamic ice production has some oscillations at roughly weekly scale, but it is not significant every year in both the break-up and freeze-up periods (not shown). The weekly oscillations in the the dynamic ice production is likely caused by the interaction between the dynamic and thermodynamic processes rather than dynamic process itself. Figure 8 shows an example of the thermal ice production during the 2012 break-up season. The diurnal cycle also exists before the break-up but its amplitude is nearly zero. Thus, it is not significant in the wavelet spectrum (Fig. 7c). Similar results are achieved with the wavelet analysis of the ice fields at YRB (Fig. 9).

The Cryosphere Discuss., https://doi.org/10.5194/tc-2017-197
Manuscript under review for journal The Cryosphere
Discussion started: 10 October 2017

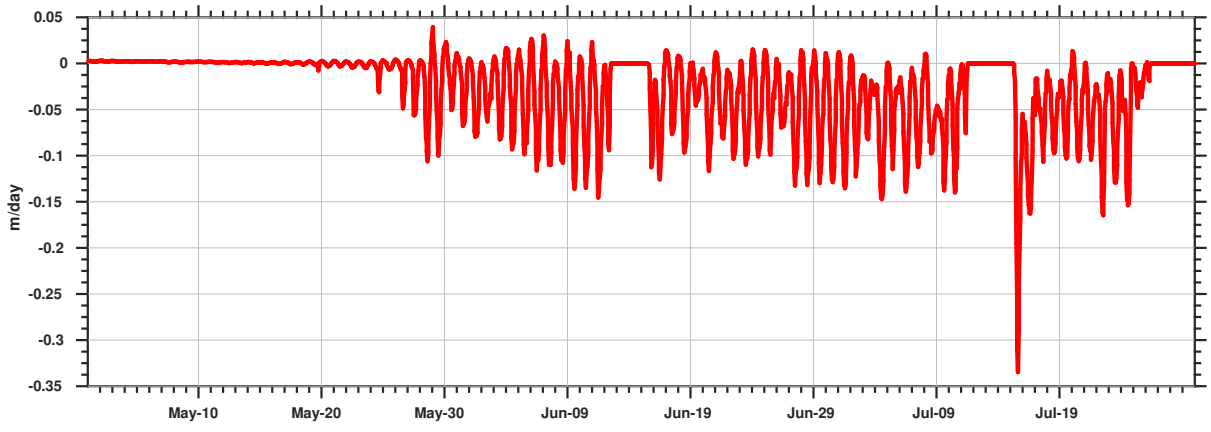

Figure 8. Diurnal cycle of thermodynamic ice production (unit: m/day) during the break-up season at YCB.

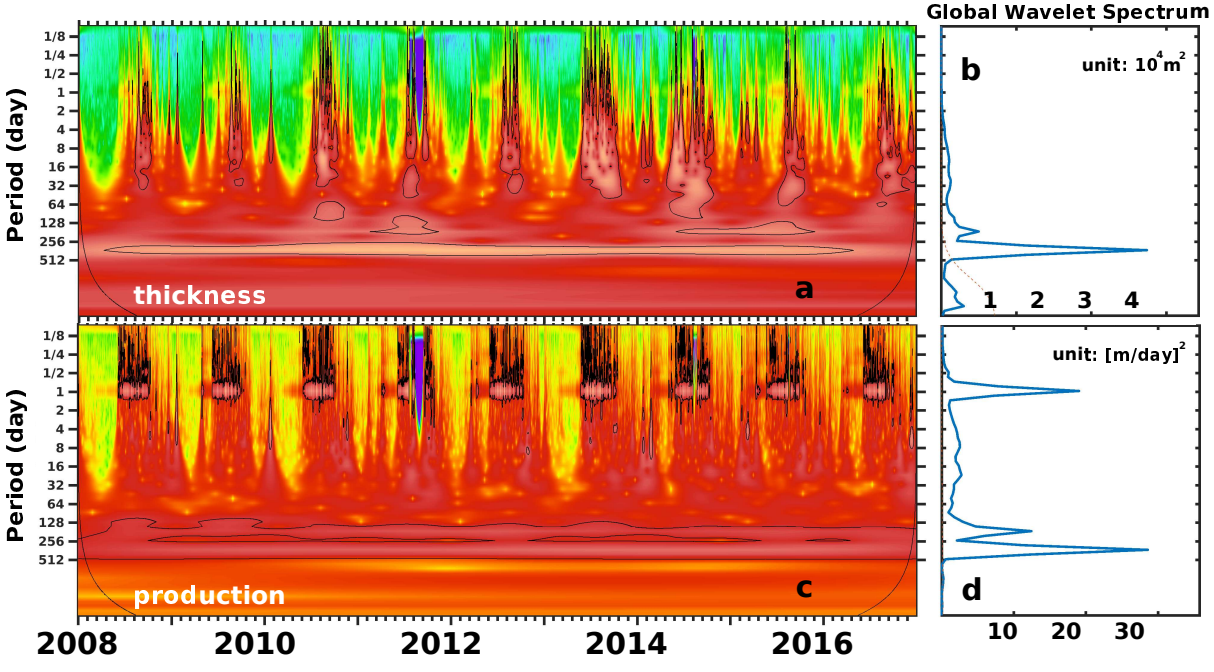

Figure 9. Same as Fig. 7 but at YRB

The thermal ice production diurnal oscillation also shows asymmetric features. For example, in 2012 (Figure 8 and 10), it can reach a melting rate of $0.1 \sim 0.15\,m\,per\,day$ ($0.04 \sim 0.1\,m\,per\,day$) during the day but will fall back to a freezing rate of $0.01 \sim 0.03\,m\,per\,day$ ($< 0.01\,m\,per\,day$) at YCB (YRB). This asymmetric feature is also seen on the season scale, more noticeable during the ice melting period than the freezing period (Figure 7c and 9c).

The Cryosphere Discuss., https://doi.org/10.5194/tc-2017-197
Manuscript under review for journal The Cryosphere
Discussion started: 10 October 2017

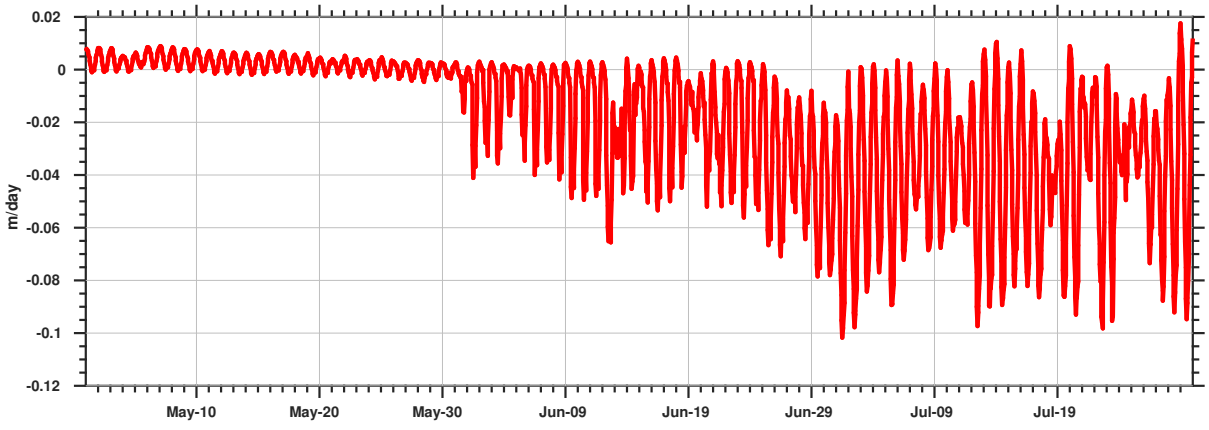

Figure 10. Same as Fig. 8 but at YRB

The Cryosphere Discuss., https://doi.org/10.5194/tc-2017-197
Manuscript under review for journal The Cryosphere
Discussion started: 10 October 2017

4 Summary and discussion

Sea ice thickness is simulated within the CAA with a relatively simple (not multi-category) sea ice model, LIM2, with both $1/4°$ and $1/12°$ resolutions from 2002 to 2016. The model can capture the ice thickness asymmetric seasonal cycle and amplitude. Even with the constrains of the resolution, simulated ice thickness still compares reasonably well with the ECCC observations at most sites. Increasing model horizontal resolution does not result in much noticeable change/improvement in sea ice thickness simulation, at least between $1/4°$ and $1/12°$. ANHA12 does show differences at WEU (Fig. 2g), but this is not related to the sea ice model physics but improvements in the local coastline, and thus the regional circulation and the dynamic component (not shown). In general, the difference is not visible. We expect model resolution to play a big role when it resolves much smaller scale, e.g., sufficient to resolve a ridge/lead. This study focuses on the large scale features, e.g., the simulations can produce reasonable spatial distribution of the thickness (very thick ice in the northern CAA, thick ice in the west-central Parry Channel and thin ice in the eastern and southern regions of CAA). With the help of the numerical model, the ice growth process can be decoupled into thermodynamic and dynamic contributions. Relatively smaller thermodynamic contribution in the winter season is found in the thick ice covered areas, with larger contributions in the thin ice covered regions (which indicates a 1D sea ice model would not be suitable there). We also find the sea thickness can vary quickly (daily to weekly) during the ice melting and formation seasons, due to the diurnal cycle in the thermodynamic ice production. The thermodynamic ice production is not symmetric for the diurnal cycle and on the seasonal scale (more pronounced during the melting period).

Landfast ice exists widely in the CAA (Melling, 2002; Galley et al., 2012; Haas and Howell, 2015; Howell et al., 2016). The sea ice model utilized here does produce zero-motion sea ice (e.g., Fig. 3d), however, more realistic physical parameterizations (e.g., Lemieux et al., 2016) are not applied in our simulations yet. Improvements are expected in both the sea ice thickness and dynamics when including such parameterizations in the future.

Another ice model physics related process is the snow depth at the surface. Both Dumas et al. (2006) and Howell et al. (2016) pointed out that the snow thickness plays a major role in a sea ice thickness simulation. The snowfall data from CORE-II has a monthly resolution, which is possibly too coarse temporally. This leads the snow depth to drop to close to zero quickly during the the first year of the simulation. This never happens with the hourly CGRF forcing, as well as other datasets with daily snowfall (Hayashida, 2017).

A large source of bias is related to the radiation fluxes (shortwave and longwave) at the atmosphere-ocean interface. The CGRF product use the GEWEX correction (more details in Smith et al. (2014)) to minimize the bias in the original output from the atmospheric model. However, it was found that this correction is not needed for years after 2011 (Paquin, 2017). A test run was done to estimate the influence of this correction. A large impact was seen in the Arctic Ocean but not over most of the CAA (not shown) except the north. Without the GEWEX correction, the model tends to simulate thinner ice with a thinner snow depth at the same time, e.g., at WEU (Fig. 11). The impact is smaller at YLT and YLT1 and negligible for the rest of the ECCC sites used in this study. Further investigation is undergoing.

The Cryosphere Discuss., https://doi.org/10.5194/tc-2017-197
Manuscript under review for journal The Cryosphere
Discussion started: 10 October 2017

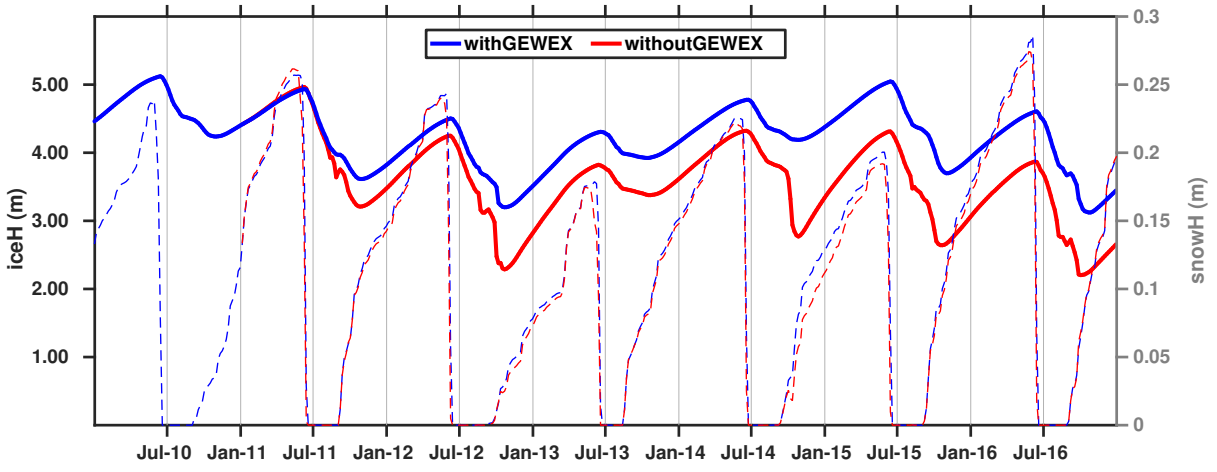

Figure 11. Simulated ice thickness (solid lines, left y-axis, unit: meters) and snow depth (dashed lines, right y-axis, unit: meters) at WEU in a ANHA4-CGRF simulation with GEWEX (blue) and without GEWEX (red) radiation flux correction

Whitefield et al. (2015) showed the heat flux carried by rivers from land into the ocean plays a role in regional sea ice simulations. Here the river water temperature is assumed to same as the simulated sea surface temperature in the grid cell where the runoff is distributed in the model. Also the salinity of the river water is assumed to be fresh, i.e., its salinity is set to zero. Another factor that may affect the local ice thickness is the tides (Luneva et al., 2015), which is not included in the simulations used in this study as well. All these factors will be considered in the future studies.

The Cryosphere Discuss., https://doi.org/10.5194/tc-2017-197
Manuscript under review for journal The Cryosphere
Discussion started: 10 October 2017

Data availability. For access to the model data contact P.G. Myers (pmyers@ualberta.ca)

Competing interests. NONE

Acknowledgements. For access to the model data contact P.G. Myers (pmyers@ualberta.ca). We gratefully acknowledge the financial and logistic support of grants from the Natural Sciences and Engineering Research Council (NSERC) of Canada. These include a Discovery Grant (rgpin 227438-09) awarded to P.G.M., Climate Change and Atmospheric Research Grants (VITALS - RGPCC 433898 and the Canadian Arctic Geotraces program - RGPCC 433848), and Polar Knowledge (432295). We are grateful to the NEMO development team and the Drakkar project for providing the model and continuous guidance, and to Westgrid and Compute Canada for computational resources. We also thank G. Smith for the CGRF forcing fields that made available by Environment and Climate Change Canada. We appreciate the Environment and Climate Change Canada New Arctic Ice Thickness Program for providing valuable sea ice thickness measurements used in this study. Greenland freshwater flux data analyzed in this study is that presented in Bamber et al. (2012) and is available on request as a gridded product. We thank NCAR/UCAR for making Dai and Trenberth Global River Flow and Continental Discharge Dataset availabile. We acknowledge WCRP/CLIVAR Ocean Model Development Panel (OMDP) for sponsing and organizing the Coordinated Ocean-sea ice Reference Experiments dataset (CORE). We also acknowledge Mercator Ocean for providing the GLORYS model output for initial and open boundary conditions. The GLORYS reanalysis project is carried out in the framework the European Copernicus Marine Environment Monitoring Service (CMEMS).

References

Agnew, T., Lambe, A., and Long, D.: Estimating sea ice area flux across the Canadian Arctic Archipelago using enhanced AMSR-E, Journal of Geophysical Research, 113, C10 011, https://doi.org/10.1029/2007JC004582, 2008.

Bailey, W. B.: Oceanographic Features of the Canadian Archipelago, J. Fish. Res. Bd. Can., 14, 731–769, https://doi.org/10.1139/f57, 1957.

Bamber, J., van den Broeke, M., Ettema, J., Lenaerts, J., and Rignot, E.: Recent large increases in freshwater fluxes from Greenland into the North Atlantic, Geophysical Research Letters, 39, L19 501, https://doi.org/10.1029/2012GL052552, 2012.

Comiso, J. C., Parkinson, C. L., Gersten, R., and Stock, L.: Accelerated decline in the Arctic sea ice cover, Geophysical Research Letters, 35, L01 703, 2008.

Dai, A., Qian, T., Trenberth, K. E., and Milliman, J. D.: Changes in continental freshwater discharge from 1948 to 2004, Journal of Climate, 22, 2773–2792, 2009.

Dickson, R., Rudels, B., Dye, S., Karcher, M., Meincke, J., and Yashayaev, I.: Current estimates of freshwater flux through Arctic and subarctic seas, Progress in Oceanography, 73, 210–230, 2007.

Drakkar Group: Eddy-permitting ocean circulation hindcasts of past decades, CLIVAR Exchanges No 42, 12, 8–10, 2007.

Dumas, J. A., Flato, G. M., and Brown, R. D.: Future projections of landfast ice thickness and duration in the Canadian Arctic, Journal of Climate, 19, 5175–5189, 2006.

Dunbar, M.: The geographical position of the North Water, Arctic, 22, 438–441, 1969.

Fichefet, T. and Maqueda, M. A. M.: Sensitivity of a global sea ice model to the treatment of ice thermodynamics and dynamics, Journal of Geophysical Research, 102, 12 609–12 646, https://doi.org/10.1029/97JC00480, http://dx.doi.org/10.1029/97JC00480, 1997.

Flato, G. M. and Brown, R. D.: Variability and climate sensitivity of landfast Arctic sea ice, Journal of Geophysical Research, 101, 25 767–25 777, https://doi.org/10.1029/96JC02431, 1996.

Galley, R. J., Else, B. G., Howell, S. E., Lukovich, J. V., and Barber, D. G.: Landfast sea ice conditions in the Canadian Arctic: 1983-2009, Arctic, pp. 133–144, 2012.

Haas, C. and Howell, S. E. L.: Ice thickness in the Northwest Passage, Geophysical Research Letters, 42, 7673–7680, https://doi.org/10.1002/2015GL065704, 2015.

Hanesiak, J. M., Barber, D. G., and Flato, G. M.: Role of diurnal processes in the seasonal evolution of sea ice and its snow cover, Journal of Geophysical Research, 104, 13 593–13 603, https://doi.org/10.1029/1999JC900054, 1999.

Hátún, H., Sandø, A. B., Drange, H., Hansen, B., and Valdimarsson, H.: Influence of the Atlantic subpolar gyre on the thermohaline circulation, Science, 309, 1841–1844, 2005.

Hayashida, H.: personal communication, 2017.

Howell, S. E. L., Tivy, A., Yackel, J. J., and McCourt, S.: Multi-year sea-ice conditions in the western Canadian Arctic Archipelago region of the Northwest Passage: 1968-2006, Atmosphere-Ocean, 46, 229–242, 2008.

Howell, S. E. L., Duguay, C. R., and Markus, T.: Sea ice conditions and melt season duration variability within the Canadian Arctic Archipelago: 1979–2008, Geophysical Research Letters, 36, L10 502, 2009.

Howell, S. E. L., Wohlleben, T., Dabboor, M., Derksen, C., Komarov, A., and Pizzolato, L.: Recent changes in the exchange of sea ice between the Arctic Ocean and the Canadian Arctic Archipelago, Journal of Geophysical Research Oceans, 118, 3595–3607, https://doi.org/10.1002/jgrc.20265, 2013.

Howell, S. E. L., Laliberté, F., Kwok, R., Derksen, C., and King, J.: Landfast ice thickness in the Canadian Arctic Archipelago from observations and models, The Cryosphere, 10, 1463, 2016.

Hu, X. and Myers, P. G.: Changes to the Canadian Arctic Archipelago Sea Ice and Freshwater Fluxes in the Twenty-First Century under the Intergovernmental Panel on Climate Change A1B Climate Scenario, Atmosphere-Ocean, 52, 331–350, https://doi.org/10.1080/07055900.2014.942592, 2014.

Hunke, E. C. and Dukowicz, J. K.: An elastic-viscous-plastic model for sea ice dynamics, Journal of Physical Oceanography, 27, 1849–1867, 1997.

Kwok, R.: Exchange of sea ice between the Arctic Ocean and the Canadian Arctic Archipelago, Geophysical Research Letters, 33, L16 501, 2006.

Kwok, R.: Sea ice convergence along the Arctic coasts of Greenland and the Canadian Arctic Archipelago: Variability and extremes (1992–2014), Geophysical Research Letters, 42, 7598–7605, 2015.

Large, W. G. and Yeager, S. G.: The global climatology of an interannually varying air–sea flux data set, Climate Dynamics, 33, 341–364, 2009.

Lemieux, J.-F., Dupont, F., Blain, P., Roy, F., Smith, G. C., and Flato, G. M.: Improving the simulation of landfast ice by combining tensile strength and a parameterization for grounded ridges, Journal of Geophysical Research: Oceans, 121, 7354–7368, 2016.

Lietaer, O., Fichefet, T., and Legat, V.: The effects of resolving the Canadian Arctic Archipelago in a finite element sea ice model, Ocean Modelling, 24, 140–152, 2008.

Luneva, M. V., Aksenov, Y., Harle, J. D., and Holt, J. T.: The effects of tides on the water mass mixing and sea ice in the Arctic Ocean, Journal of Geophysical Research: Oceans, 120, 6669–6699, 2015.

Madec, G. and the NEMO team: NEMO ocean engine, Note du Pôle de modélisation, Institut Pierre-Simon Laplace (IPSL), France, No 27, ISSN No 1288-1619, 2008.

Marshall, J., Kushnir, Y., Battisti, D., Chang, P., Czaja, A., Dickson, R., Hurrell, J., McCartney, M., Saravanan, R., and Visbeck, M.: North Atlantic climate variability: phenomena, impacts and mechanisms, International Journal of Climatology, 21, 1863–1898, 2001.

Masina, S., Storto, A., Ferry, N., Valdivieso, M., Haines, K., Balmaseda, M., Zuo, H., Drevillon, M., and Parent, L.: An ensemble of eddy-permitting global ocean reanalyses from the MyOcean project, Climate Dynamics, pp. 1–29, https://doi.org/10.1007/s00382, 2015.

Maslanik, J., Stroeve, J., Fowler, C., and Emery, W.: Distribution and trends in Arctic sea ice age through spring 2011, Geophysical Research Letters, 38, https://doi.org/10.1029/2011GL047735, 2011.

Melling, H.: Sea ice of the northern Canadian Arctic Archipelago, Journal of Geophysical Research, 107, 3181, 2002.

Melling, H., Gratton, Y., and Ingram, G.: Ocean circulation within the North Water polynya of Baffin Bay, Atmosphere-Ocean, 39, 301–325, https://doi.org/10.1080/07055900.2001.9649683, 2001.

Melling, H., Agnew, T., Falkner, K. K., Greenberg, D. A., Lee, C. M., Münchow, A., Petrie, B., Prinsenberg, S. J., Samelson, R. M., and Woodgate, R. A.: Fresh-water fluxes via Pacific and Arctic outflows across the Canadian polar shelf, Arctic-Subarctic Ocean Fluxes: Defining the Role of the Northern Seas in Climate, pp. 193–247, 2008.

Paquin, J.-P.: personal communication, 2017.

Parkinson, C. L. and Cavalieri, D. J.: Arctic sea ice variability and trends, 1979–2006, Journal of Geophysical Research, 113, C07 003, 2008.

Parkinson, C. L. and Comiso, J. C.: On the 2012 record low Arctic sea ice cover: Combined impact of preconditioning and an August storm, Geophysical Research Letters, 40, 1356–1361, https://doi.org/10.1002/grl.50349, 2013.

Parkinson, C. L., Cavalieri, D. J., Gloersen, P., Zwally, H. J., and Comiso, J. C.: Arctic sea ice extents, areas, and trends, 1978–1996, Journal of Geophysical Research, 104, 20 837–20 856, 1999.

Peterson, I., Hamilton, J., Prinsenberg, S., and Pettipas, R.: Wind-forcing of volume transport through Lancaster Sound, Journal of Geophysical Research, 117, C11 018, https://doi.org/10.1029/2012JC008140, 2012.

Pizzolato, L., Howell, S. E. L., Derksen, C., Dawson, J., and Copland, L.: Changing sea ice conditions and marine transportation activity in Canadian Arctic waters between 1990 and 2012, Climatic Change, 123, 161–173, https://doi.org/10.1007/s10584-013-1038-3, 2014.

Pizzolato, L., Howell, S. E. L., Dawson, J., Laliberté, F., and Copland, L.: The influence of declining sea ice on shipping activity in the Canadian Arctic, Geophysical Research Letters, 43, 2016.

Prinsenberg, S. J. and Hamilton, J.: Monitoring the volume, freshwater and heat fluxes passing through Lancaster Sound in the Canadian Arctic Archipelago, Atmosphere-Ocean, 43, 1–22, 2005.

Renka, R. J.: Multivariate interpolation of large sets of scattered data, ACM Transactions on Mathematical Software, 14, 139–148, https://doi.org/10.1145/45054.45055, 1988.

Rhein, M., Kieke, D., Hüttl-Kabus, S., Roessler, A., Mertens, C., Meissner, R., Klein, B., Böning, C. W., and Yashayaev, I.: Deep water formation, the subpolar gyre, and the meridional overturning circulation in the subpolar North Atlantic, Deep Sea Research Part II: Topical Studies in Oceanography, 58, 1819–1832, 2011.

Semtner Jr, A. J.: A model for the thermodynamic growth of sea ice in numerical investigations of climate, Journal of Physical Oceanography, 6, 379–389, 1976.

Serreze, M. C., Holland, M. M., and Stroeve, J.: Perspectives on the Arctic's shrinking sea-ice cover, Science, 315, 1533–1536, 2007.

Smith, G. C., Roy, F., Mann, P., Dupont, F., Brasnett, B., Lemieux, J.-F., Laroche, S., and Bélair, S.: A new atmospheric dataset for forcing ice–ocean models: Evaluation of reforecasts using the Canadian global deterministic prediction system, Quarterly Journal of the Royal Meteorological Society, 140, 881–894, 2014.

Sou, T. and Flato, G.: Sea ice in the Canadian Arctic Archipelago: Modeling the past (1950–2004) and the future (2041–60), Journal of Climate, 22, 2181–2198, 2009.

Stroeve, J., Serreze, M., Drobot, S., Gearheard, S., Holland, M., Maslanik, J., Meier, W., and Scambos, T.: Arctic sea ice extent plummets in 2007, Eos, Transactions American Geophysical Union, 89, 13–14, 2008.

Torrence, C. and Compo, G. P.: A practical guide to wavelet analysis, Bulletin of the American Meteorological society, 79, 61–78, 1998.

Veleda, D., Montagne, R., and Araujo, M.: Cross-Wavelet Bias Corrected by Normalizing Scales, Journal of Atmospheric and Oceanic Technology, 29, 1401–1408, https://doi.org/10.1175/JTECH, 2012.

Vellinga, M. and Wood, R. A.: Global climatic impacts of a collapse of the Atlantic thermohaline circulation, Climatic change, 54, 251–267, 2002.

Whitefield, J., Winsor, P., McClelland, J., and Menemenlis, D.: A new river discharge and river temperature climatology data set for the pan-Arctic region, Ocean Modelling, 88, 1–15, https://doi.org///dx.doi.org/10.1016/j.ocemod.2014.12.012, 2015.